PCCP

Cite this: *Phys. Chem. Chem. Phys.*, 2012, **14**, 15953–15962

www.rsc.org/pccp

PERSPECTIVE

Doping $BiFeO_3$: approaches and enhanced functionality

Chan-Ho Yang,[a] Daisuke Kan,[b] Ichiro Takeuchi,[c] Valanoor Nagarajan[d] and Jan Seidel*[d]

Received 4th September 2012, Accepted 10th October 2012
DOI: 10.1039/c2cp43082g

$BiFeO_3$ is one of the most studied multiferroic materials. Both its magnetic and ferroelectric properties can be influenced by doping. A large body of work on the doped material has been presented in the past couple of years. In this paper we provide a perspective on general doping concepts and their impact on the material's functionality.

1. Introduction

Bismuth ferrite is one of the rare multiferroic compounds in which ferroelectricity and magnetism coexist at room temperature. Both its antiferromagnetic and ferroelectric transition temperatures are well above room temperature (643 K and 1100 K, respectively). It has been synthesized in bulk and thin film form. Considerable attention has been devoted to this material because of its fundamental coupling phenomena of the multiple order parameters and practical applications for magnetoelectric devices based on electrically controlled magnetism.[1–3] Bulk $BiFeO_3$ (BFO) has a rhombohedral symmetry (space group *R*3*c*) and its ferroelectric polarization of $\sim 100\ \mu C\ cm^{-2}$ is oriented along one of the $\langle 111 \rangle$ pseudocubic axes.[4–7] The perovskite-type unit cell (see Fig. 1) has a lattice parameter of $a = 3.965$ Å and a rhombohedral angle of $\sim 89.3–89.48°$ at room temperature.[8] The polarization is mainly caused by the Bi^{3+} lone pair ($6s^2$ orbital), *i.e.* the polarization originates mostly from the A-site while the magnetization comes from Fe^{3+}, *i.e.* the B-site. The material has large merits in terms of epitaxial growth of high quality thin films as well as its multiferroic properties at room temperature. Epitaxial growth along with versatile domain engineering by varying lattice parameters of substrates, orientations and miscut angles have been extensively studied,[9–12] which provide a base for reliable research on ferroelectric and magnetoelectric properties of $BiFeO_3$. Moreover, such studies are not limited to dielectric properties but expanding to electronic and ionic conduction properties as well. It has been reported that $BiFeO_3$ undergoes a structural transition at high temperature to a cubic phase which shows metallic conduction as well as closing of the optical band gap.[13] Such a metallic conduction of $BiFeO_3$ has also been found in circumstances of hydrostatic pressure.[14] Moreover, a large enhancement of electronic conduction at ferroelectric domain walls has been discovered.[15–17] A more active way to improve the physical properties or/and induce unexpected phenomena relies on substituting different ions into the A-site or B-site of bismuth ferrite. By taking into account that high T_c superconductivity[18] and colossal magnetoresistance[19] were created as a result of hole carrier doping into the parent antiferromagnetic insulators and that phase competition at the morphotropic phase boundary of *e.g.* ferroelectric $Pb(Zr,Ti)O_3$ brings about large enhancement of dielectric and piezoelectric properties,[20,21] we are motivated to study doping-driven manifestations of novel properties and enhanced functionality. In the present perspective, we first discuss the fundamental solid state phenomena that shape the physical and chemical properties of BFO. This is necessary to understand the expectations from generic doping effects on

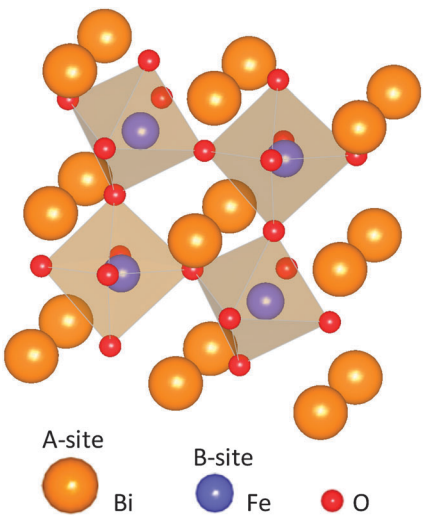

Fig. 1 The perovskite crystal structure of $BiFeO_3$.

[a] *Department of Physics, and Institute for the NanoCentury, Korea Advanced Institute of Science and Technology (KAIST), Daejeon 305-701, Republic of Korea*
[b] *Institute for Chemical Research, Kyoto University, Uji City 611 0011, Japan*
[c] *Department of Materials Science and Engineering, University of Maryland, College Park, Maryland 20742, USA*
[d] *School of Materials Science and Engineering, The University of New South Wales, Sydney, New South Wales 2052, Australia. E-mail: jan.seidel@unsw.edu.au*

bismuth ferrite especially focusing on the multiferroic aspect of electronic conduction and magnetism. Finally, we introduce recent progress in the field of doped BFO and provide an outlook on future trends.

2. Bismuth ferrite – solid state chemistry and band structure

In order to fully appreciate the effect of dopants on the physical properties of BFO we need to first consider the solid state properties of BFO itself with a focus on key aspects of relevance to doping.

2.1 Structure–properties relations: role of the perovskite structure

Perovskite (ABO_3) bismuth ferrite has Fe^{3+} ions at B-sites surrounded by six neighboring oxygen anions forming FeO_6 octahedra which are connected to one another by sharing their corners. Empty spaces, *i.e.* A-sites, between the FeO_6 backbones are occupied by Bi^{3+} ions. Such perovskite structures are formed by occupying the B-sites usually with transition metal ions and by filling the A-sites with trivalent rare-earth ions or divalent alkali-earth ions. It is believed that physical properties of perovskite compounds are mainly attributed to the transition metal ions located at the B-sites and electronic band formation as well as electronic conduction are largely affected by the chemical bonding between Fe^{3+} and oxygen anions.

For a perovskite structure to be stable, ionic radii of constituent elements should match well. The Goldschmidt tolerance factor, defined as $t = \frac{r_A + r_O}{\sqrt{2}(r_B + r_O)}$, can be introduced to indicate the extent of the harmony between the ionic radii. r_A, r_B, and r_O stand for ionic radius of A-site, B-site, and oxygen ions, respectively, and these ionic radii can be obtained in Shannon's tables on effective ionic radii.[22] Ideally, the tolerance factor should be equal to or less than one. For BFO it is 0.88. The smaller the tolerance factor, the more severely is the buckling between the oxygen octahedra. This is due to the fact that the smaller A-site ions cannot fill the empty space fully and instead the octahedra are tilted, shrinking the space. As a result, the bond angle of Fe^{3+}–O^{2-}–Fe^{3+} deviates from 180 degrees. For $BiFeO_3$, the octahedral tilt is $\sim$11–14° around the polar [111] axis, with the directly related Fe–O–Fe angle being 154–156°.[23] The Fe–O–Fe angle is crucial because it controls both the magnetic exchange and orbital overlap between Fe and O, *i.e.* it determines the magnetic and conduction properties. In this regard, the A-site substitutions by some ions with smaller ionic radius would induce more buckling in the Fe–O–Fe bond angle accompanying a smaller tolerance factor leading to a more insulating character. Since most lanthanide rare-earth trivalent ions have a smaller ionic radius than the Bi^{3+} ion, the substitutions are expected to bring about a more insulating behavior in bismuth ferrite. Experimental estimation of the bond angle bending can be made through detection of a superlattice peak indicative of the extent of cooperative tilt of antiferrodistortive octahedra. Glazer has described 23 different octahedron tilt systems of the normal perovskite structure under the assumption of rigid octahedra. The rhombohedral structure of $BiFeO_3$ corresponds to a Glazer tilt system of $a^-a^-a^-$ which induces a superlattice peak at (1/2 1/2 1/2) reciprocal lattice positions.[24] The intensity of the superlattice peak can have the role of an order parameter to indicate the extent of band width and bond angle tilt. Large deviations in the tolerance factor from one by substitutions of too small A-site ions would make the chemical structure unstable, which corresponds to the case that late lanthanide based perovskites tend to be hexagonal perovskites rather than a normal perovskite.

2.2 Electronic structure

$BiFeO_3$ has bismuth ions (Bi^{3+}) at the A-sites, which is different from normal perovskites, as they usually contain rare earth ions at the A-site positions. Typical rare earth ions have partially filled f-shells which are spatially located closer to the core region and are protected by outer shells of stable 5s and 5p orbitals. Accordingly, rare earth ions are inert without producing strong chemical bonds with neighboring oxygen ions. Their main roles are to occupy the empty spaces between oxygen octahedra influencing physical properties indirectly by controlling the bond angle and to affect band filling by donating electrons into the B-site ions. However, the Bi^{3+} ions of $BiFeO_3$ have 6s electrons at the outer shell, resulting in a reactive nature in terms of spatial positions and electron energy levels, which may either produce covalent bonding with neighboring oxygen ions (Bi 6sp–O 2p)[25] or make 6s lone pairs.[26] Regardless of these somewhat controversial views on the roles of the 6s electrons, either way leads to the conclusion that $BiFeO_3$ has electric dipole moments and moreover they are aligned to produce a ferroelectric polarization. Such an origin of ferroelectricity for the $BiFeO_3$ is quite distinct from other conventional displacive ferroelectrics such as $BaTiO_3$ which have electric dipole moments arising from d^0-ness of the transition metal ions. Hybridization between the empty d orbital and the filled oxygen 2p orbital would generate cation off-centering because the electronic energy can be lowered through filling only the hybridized bonding state.[27] However, the Fe^{3+} has five electrons in d orbitals and it is inevitable that the hybridization should fill not only the bonding state but also the unstable anti-bonding state. There is no reason that such off-centering happens at the expense of elastic deformation without electronic energy gain.

Regarding the magnetic properties of $BiFeO_3$, we have to focus on the d orbitals. When a Fe^{3+} ion is located at the center of an oxygen octahedron, the degenerate d orbital states are split into a t_{2g} triplet state and an e_g doublet state separated by the crystal field splitting energy ($10D_q$). All the five electrons in d orbitals have parallel spins producing 5 μ_B per Fe^{3+} ion. The localized character of the 3d orbital is strong enough to produce such a local magnetic moment through on-site electron correlation while it is not so strong as to prohibit inter-site exchange interaction which is required to induce reasonably high ordering temperatures. In fact, the d orbitals do not have direct overlap spatially with neighboring Fe^{3+} sites. Exchange interaction for magnetic ordering can be obtained through oxygen 2p orbitals. Exact half filling of d orbitals with 5 electrons makes for spherical symmetry in

the d orbital cloud and thereby it is expected that the magnetic moment of a Fe^{3+} ion interacts with six neighboring local spins *via* the same exchange integral. The type of effective exchange interaction and its strength can be predicted by Goodenough–Kanamori–Anderson rules.[28,29] For the d^5–d^5 case, the dominant interaction is between neighboring half filled e_g orbitals through oxygen 2p σ-bonding. Exchange interaction between half-filled orbitals is antiferromagnetic, according to the Goodenough–Kanamori–Anderson rules. Intermixing of the two neighboring orbitals through hopping and consequently energy lowering are allowed for antiferromagnetic spin arrangement, whereas they are prohibited for the ferromagnetic case because of the Pauli exclusion principle. It is also understood that the exchange interaction is strong because a large overlap integral is predicted between the e_g orbital and an oxygen 2p orbital aligned along the bonding axis. On these grounds, we can understand why $BiFeO_3$ has a G-type antiferromagnetic order producing a magnetic peak at (1/2 1/2 1/2) pseudocubic position together with a quite high Néel temperature at 640 K. With this background on the relation of chemical bonding to the magnetic and electric order, we move on to the band structure.

2.3 Band structure, bandwidth and band filling

$BiFeO_3$ is a charge-transfer-type insulator where on-site Coulomb repulsion is so strong that the lower Hubbard band of the d-orbital becomes lower than the band of the oxygen 2p orbital. Such an electronic structure is often found in transition metal oxide perovskites and related structures consisting of late 3d elements as like Fe, Co, Ni, and Cu ions which show rather strong localized character of the d-orbital electrons. In the case, the conduction band for the perspective of one electron band picture is mainly composed of the d orbital state and whereas the valence band consists of the oxygen 2p state dominantly.[30] The extent of band dispersion so-called band width is represented by the effective mass of carriers and directly related to hopping integral ($t_{pd}^{\alpha\beta}$): $t_{pd}^{\alpha\beta} = \int \varphi_{2p}^{\alpha *}(r)h(r)\varphi_{3d}^{\beta}(r)dr$, where $h(r)$ implies a one-body Hamiltonian, and $\varphi_{2p}^{\alpha}(r)$ and $\varphi_{3d}^{\beta}(r)$ are a wave function of the 2p αth orbital and the 3d βth orbital, respectively. A larger hopping integral induces a wider band width and, as a result, the optical band gap is decreased and eventually metallic character is enhanced. To get larger hopping integral ($t_{pd}^{\alpha\beta}$), the relevant orbitals should overlap more intensively without cancelling due to anti-symmetric phase terms of the wave functions. The overlap integral depends sensitively on not only bond length but also bond angle.

Whilst the link between crystallographic structure and polar (electromechanical) properties is common to all ferroelectrics, in the case of bismuth ferrite severe buckling of the bond angle has an equally critical role in the magnetic properties. It creates an anti-symmetric magnetic interaction, the so-called Dzyaloshinskii–Moriya (DM) interaction ($\vec{D}_{ij}\cdot\vec{S}_i \times \vec{S}_j$), which becomes important in addition to the normal isotropic symmetric exchange interaction ($J_{ij}\vec{S}_i\cdot\vec{S}_j$). The DM interaction originates from spin–orbit interaction and it would induce non-collinear spin states including canted antiferromagnetism. The DM coefficient of $\vec{D}_{ij}$ can be ignored through symmetry consideration when the oxygen anion is located on the line ($\vec{r}_{ij}$) connecting the *i*th Fe^{3+} ion with a neighboring *j*th one, *i.e.*, the bond angle is 180°. Otherwise, the DM coefficient becomes considerable in proportion to $\vec{D}_{ij} \propto \vec{e} \times \vec{r}_{ij}$ where $\vec{e}$ stands for the deviation vector of the oxygen anion from the line of $\vec{r}_{ij}$.[31,32] Although the magnitude of the DM coefficient is one order of magnitude smaller than the symmetric exchange interaction in the $BiFeO_3$ compound, we cannot fully exclude the possibility of net magnetism due to canted antiferromagnetism. Moreover, severe tilting by control of epitaxial strain[33,34] as well as chemical pressure provides a pathway to a real multiferroic where ferroelectricity and ferromagnetism coexist.

3. General doping concepts

In the following we will discuss A-site, B-site and oxygen substitution of $BiFeO_3$ and give specific examples for each case.

3.1 A-site substitution

A-site substitution refers to the case that the Bi^{3+} ions are replaced by the other ions. Since the electronic levels of A-site ions are located far away from the Fermi level, the A-site substitution can influence the band structure indirectly. Effects of the A-site substitutions on electronic band structure can be described in terms of control of band width and control of band filling. A-site substitutions by some ions with smaller ionic radius can induce more buckling in the Fe–O–Fe bond angle accompanying a smaller tolerance factor leading to a more insulating character. Carrier-doping-driven physical properties in other perovskites include high-T_c superconductivity and colossal magnetoresistance induced when divalent ions are inserted into the trivalent A-site ions in the parent antiferromagnetic insulators. In this respect, replacing the Bi^{3+} by divalent ions like Ca^{2+} and Sr^{2+} might realize novel conducting states of hole-doped $BiFeO_3$, unless other dopants like oxygen vacancies are produced. Because of charge neutrality, some of the ligand levels in the valence band will be vacant, *i.e.*, hole carriers are introduced by control of band filling. On the other hand, substitution of Ce^{4+} ions is known to produce electron carriers.

Some examples of A-site doping

A. Electronic structure modulation via A-site substitution: the case of Ca-doping. Ca doping of BFO leads to strong similarity of the phase diagram to the ones of high-T_c superconductors and colossal magnetoresistive manganites where a competition between energetically similar ground states is introduced by hole doping (Fig. 2).[35]

Control of the conductive properties by band-filling was observed in Ca-doped BFO. Application of an electric field enabled this control to the extent that a p–n junction can be formed, erased and inverted in this material.

A 'dome-like' feature in the phase diagram is observed around a Ca concentration of 1/8, where a new pseudo-tetragonal phase appears and the electric modulation of conduction is found to be largest. Conductive-AFM measurements reveal that the material exhibits resistive switching and that sub sequent application of electric fields can reverse the effect.

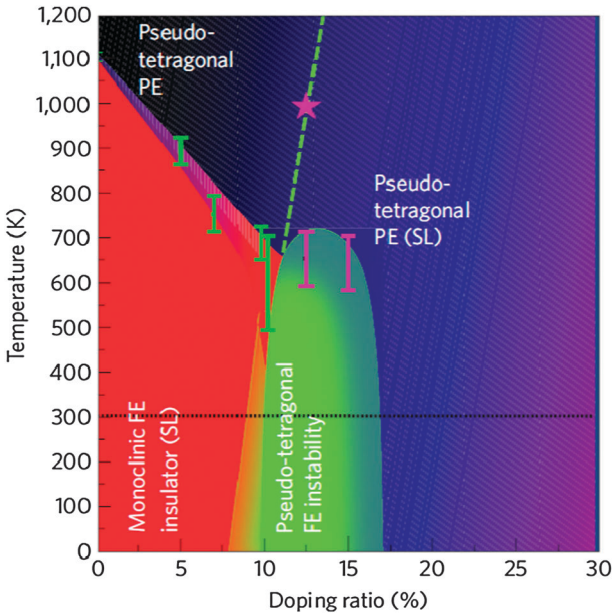

Fig. 2 Phase diagram of $Bi_{1-x}Ca_xFeO_{3-\delta}$ films grown on (001) $SrTiO_3$.

The observed reversible modulation of electric conduction accompanied by the modulation of the ferroelectric state is a consequence of the spatial movement of naturally produced oxygen vacancies under an electric field that acts as donor impurities to compensate Ca acceptors and maintain a highly stable Fe^{3+} valence state. This conductor–insulator transition can be understood in terms of the competition between a mobility edge and the Fermi energy through band-filling control. This observation might lead to new concepts for merging magnetoelectrics and magnetoelectronics at room temperature by combining electronic conduction with electric and magnetic degrees of freedom.[36–39] This doping concept of Ca and Mn, among others, might also be applicable to domain walls in $BiFeO_3$.[40]

B. Tuning electromechanical properties via rare-earth doping: in search of new morphotropic phase boundaries. Chemical substitutions have been recognized to be a useful way to tune materials to be at their structural boundary where different structural phases with a close energy level can coexist and as a consequence colossal response in reaction to weak external stimuli such as temperature, electric field, or magnetic field is often displayed. A good example is the morphotropic phase boundary (MPB) observed for Pb-based ferroelectrics[41–45] at which a gigantic piezoelectric response is observed. Thus the composition tuning through A or B site substitution in perovskite ferroelectrics has been considered to be one well-known route for achieving a MPB with enhanced functional properties.

While it has been widely accepted that BFO[7,46,47] is an environmentally friendly (Pb free) ferroelectric with the added functionality of room-temperature multiferroicity, the fact that it suffers from high-leakage current, large coercive fields as well as possession of electromechanical coefficients much smaller than traditional Pb-based piezoelectrics has motivated chemical substitutions into BFO so that they emulate the MPB behaviors for Pb-based piezoelectrics.

Here we briefly review recent findings[48–50] focused on structural and electromechanical properties of rare-earth (RE^{3+} = La^{3+}, Sm^{3+} and Dy^{3+}) substituted BFO by means of a thin-film composition spread technique. The ionic radii of these trivalent ions with the coordination number of twelve are Bi^{3+}(1.36 Å) ~ La^{3+}(1.36 Å) > Sm^{3+}(1.28 Å) > Dy^{3+} (1.24 Å).[51] Following the solid-state arguments of perovskite stability, and given the close link between crystallographic structure, polarization orientation and the electromechanical response in ferroelectrics, it is no surprise that the substitution-induced evolution in the ferroelectric, dielectric and piezoelectric properties is strongly dependent on the ionic size of the substitution elements. However what is remarkable is that a universality in terms of the effective A-site radius was found for the case of rare-earth doped BFO thin films in 2010. A structural transition from the undoped ferroelectric rhombohedral phase to an orthorhombic phase exhibiting a double polarization hysteresis loop and substantially enhanced electromechanical properties were found to occur independent of the RE dopant species, controlled by the average ionic radius of the A-site cation. Using the first principles calculations we proposed the origin of the double hysteresis loop and the concomitant enhancement in the piezoelectric coefficient to be an electric-field-induced transformation from a paraelectric orthorhombic phase to the polar rhombohedral phase. Fig. 3 below is a universal phase diagram that was proposed following the above finding.

Further investigations on the role of ionic size of the dopant revealed not only a change in the concentration of the rare-earth dopant required for inducing the phase boundary but also a strong effect on the pathway taken by the system. This marked difference in the phase transition behavior is

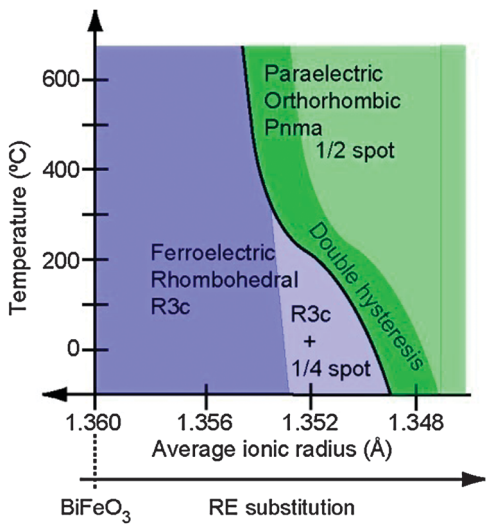

Fig. 3 Universal phase diagram of RE-substituted $BiFeO_3$ films. The black line represents the structural phase boundary between the rhombohedral (in blue) and the orthorhombic (in green) structural phases. At the lower temperature side, the 1/4{011} spot due to the minority phase with a $PbZrO_3$-type structure is observed in the region in light blue. The double hysteresis loop behavior emerges in the region in dark green.

attributed to the unit cell dimension of the rare-earth orthoferrite phase. In the case of smaller rare-earths such as Sm it was found to be $\sqrt{2}a_{pc} \times \sqrt{2}a_{pc} \times 2a_{pc}$ while for rare-earth La (which has much larger ionic radii) it is $a_{pc} \times a_{pc} \times 2a_{pc}$. For smaller rare-earths an abrupt drop in d_{001_pc} is observed attributed to the change in the dimensions of the unit cell from the $a_{pc} \times a_{pc} \times a_{pc}$ for the rhombohedral phase to $\sqrt{2}a_{pc} \times \sqrt{2}a_{pc} \times 2a_{pc}$ for the orthorhombic phase. For example, in the case of Sm-doped BFO, across the boundary the unit cell volume (in terms of the pseudo-cubic perovskite unit cell) is decreased by 1.2% due to the abrupt drop in d_{001_pc}. In contrast, the fundamental unit-cell for La-substituted BFO remains unchanged at $a_{pc} \times a_{pc} \times a_{pc}$ across the structural boundary, although the lattice parameter along the $[001]_{ortho}$ axis is doubled as evidenced by the presence of 1/2{010} XRD spots.[50]

The size of the rare-earth dopant controls not just the pathway of the structural transitions. Indeed it has also a significant role in the structural phase stability, as verified by the temperature dependence of the lattice parameter, 1/4{011} and 1/2{010} XRD superstructure spot intensities. It was determined that the 1/4{011} (referred to as 1/4) spot arises from the presence of minority phase with a $PbZrO_3$-type structure and that the 1/2{010} (1/2) spot results from the cell-doubled orthorhombic structural phase. The temperature dependence of these structural properties revealed that the stronger chemical pressure due to the substitution moves the 1/4 spot region into the lower composition side, and in the same vein, the composition region where the 1/2 spot intensity is seen is extended toward lower composition and lower temperature region with decreasing ionic size of the RE elements. Based on these observations, schematic phase diagrams as a function of the ionic size of the RE-dopant were constructed. For the smaller RE-substituted BFO[10] (RE = Dy and Sm) (Fig 4a), the 1/2 structural phase with dimensions of $\sqrt{2}a_0 \times \sqrt{2}a_0 \times 2a_0$ is stabilized due to the strong chemical pressure. We define x and x′ as a substitution composition at which the 1/4 and 1/2 spot intensities begin to appear at room temperature, respectively. For lower temperatures, the appearance of the 1/4 phase (in the composition region between x and x′ at room temperature) appears to "bridge" the rhombohedral phase to the orthorhombic one. Beyond x′ at room temperature, the orthorhombic phase begins to emerge. As temperature is increased, the 1/4 spot disappears, and the orthorhombic phase is located right next to the rhombohedral phase in the diagram.

We extended the phase diagram for the strong chemical pressure case (Fig. 4a) to the negligibly weak chemical pressure case (RE = La) by simply shifting the 1/4 spot region and the structural boundary into the higher substitution composition and higher temperature regions. The difference from the strong chemical pressure case (RE = Sm and Dy) is that the 1/2 structural phase is the orthorhombic (or tetragonal-like) phase with dimensions of $a_0 \times a_0 \times 2a_0$, although the 1/2 structural phase is still bridged by the 1/4 phase to the rhombohedral phase at lower temperature region. In the higher temperature region where the 1/4 spot disappears, the 1/2 phase remains right adjacent to the rhombohedral phase in the diagram.

The ferroelectric and piezoelectric properties also display RE-dependent concomitant changes across the structural boundary. Fig. 4a displays the evolution of room-temperature *P–E* hysteresis loops across the structural boundary for the RE = Sm and La cases. The compositions for each case are chosen such that they capture the representative characteristics of the evolution in sufficient composition ranges. The difference in Sm and L-doped BFO thin film behaviors is exemplified by the loop for La 27%, where the double hysteresis behavior becomes less pronounced and the *P–E* loop is likely the one characteristic for the paraelectric phase. This behavior for RE = La is independently confirmed by the dielectric constant *vs.* electric field curves[50] which did not show clear quadruple-humped loops observed for the orthorhombic phase adjacent to the boundary in Sm-substituted BFO. Similarly, the variation in electromechanical properties strongly depends on the RE ionic size.

Fig. 5b and c plot the piezoelectric coefficient d_{33} values as a function of the dopant composition for the RE = Dy^{3+} and

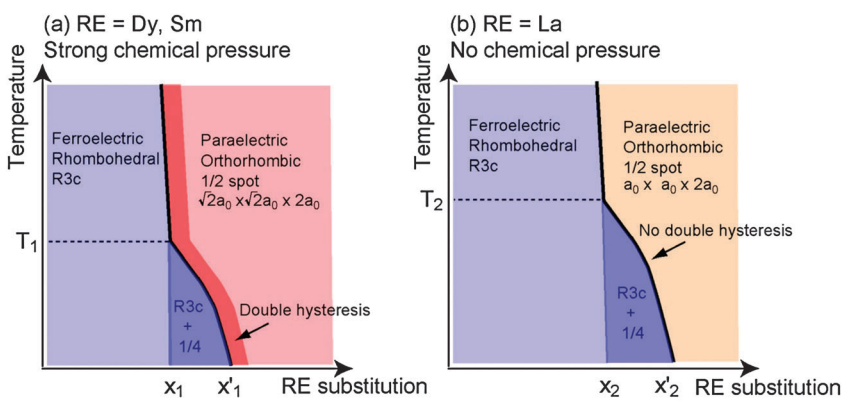

Fig. 4 Schematic phase diagram for RE-substituted BFO in the presence of (a) the strong chemical pressure due to RE substitutions (RE = Dy and Sm) and (b) no (or negligibly weak) chemical pressure (RE = La). The subscripts 1 and 2 denote the strong chemical pressure case (RE = Sm and Dy) and no chemical pressure case (RE = La), respectively. In the diagram, T_1 and T_2 denote the highest temperature at which the 1/4 spot appears. x_1 and x'_1 (x_2 and x'_2 for the RE = La case) stand for the compositions at which the 1/4 spot appears and disappears at room temperature. The stronger chemical pressure shifts the 1/4 spot region into lower temperature and lower composition side ($T_1 < T_2$, $x_1 < x_2$, $x'_1 < x'_2$).

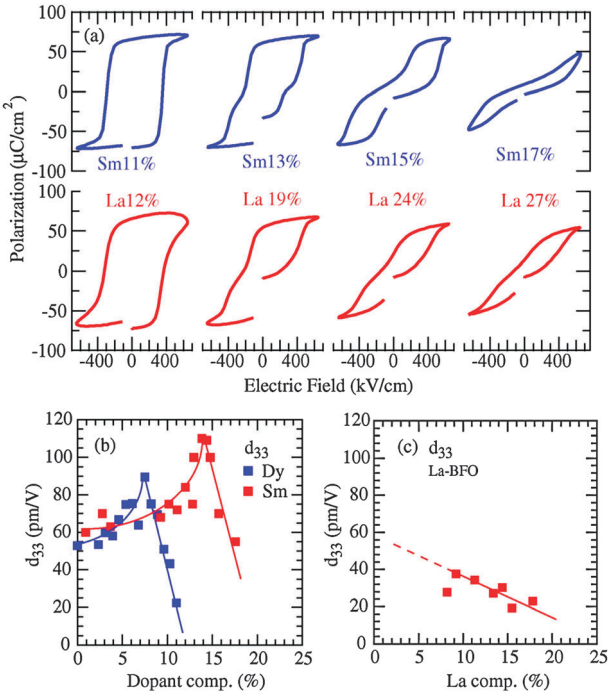

Fig. 5 (a) Evolution in the room temperature *P–E* hysteresis loops across the structural transition for Sm- (upper panels) and La-substituted BFO thin films (lower panels). All loops were acquired at 25 kHz. (b and c) Piezoelectric coefficient d_{33} at 400 kV cm^{-1} as a function of RE substitution for (b) RE = Dy^{3+} and Sm^{3+}, and (c) RE = La^{3+} cases. The lines are a guide to the eye to highlight the peaking behavior of d_{33}.

Sm^{3+}, and RE = La cases, respectively. For the smaller RE cases, an enhancement in the piezoelectric response at the boundary composition is observed with the value reaching 110 pm V^{-1} for RE = Sm.[48] In contrast, for the RE = La case, there is no enhancement in d_{33} in spite of a structural transition at 23%. The d_{33} value shows a monotonous decrease (down to almost zero) as one approaches the phase boundary, revealing that there is no distinct increase in the electromechanical properties.

The fact of no enhancement in d_{33} associated with less pronounced double hysteresis behavior for the RE = La case suggests that a structural platform required for the electric-field transformation is absent, which is probably caused by the RE-dependent orthorhombic phase.[12] In fact, the electron diffraction studies[50] revealed that only the smaller RE-substituted BFOs exhibit the nano-scale phase coexistence of the parent rhombohedral ferroelectric phase, antipolar PZO-like phase and cell-doubled orthorhombic paraelectric phase at the structural boundary, while for the RE = La case the signature of the phase coexistence is distinctly weak as verified by the very faint 1/2 superstructure spot arising from the orthorhombic phase. This leads to the conclusion that the nano-scale phase coexistence acts as a facile platform for the theoretically-predicted electric-field-induced structural transformation and that this is why no enhanced properties are seen for the RE = La case. We also find that the chemical substitution plays a critical role in determining the direction along which the enhanced properties including the dominant piezoelectric coefficient are observed. This is due to the substitution-induced continuous rotation in the polarization vector from the [111] direction for pure BFO to the [001] direction for RE-substituted BFO at the MPB, which explains why the double hysteresis behavior with enhanced piezoelectric coefficient d_{33} is prominently observed only for the (001) oriented film.[52]

3.2 B-site substitution

The B-site substitutions are made by replacing the Fe^{3+} ions by other transition metal ions. Since the conduction band of $BiFeO_3$ is related to the d orbital state of the Fe^{3+} ion, B-site substitutions can have a strong influence on physical properties by changing the electronic structure near the Fermi level. First of all, it is important to consider whether the substitution produces ordered structures of the dopant ions or random distributions. This issue is strongly related to the ionic radius of the dopant. Large mismatch of the Fe^{3+} ionic radius and the dopant ionic radius can induce an ordered structure particularly in heavy doping cases. A good example of such a case is a double perovskite of the Sr_2FeMoO_6 compound which shows ferromagnetism and metallic conduction.[53] Since the charge valence state and ionic radius of the substituent Mo^{5+} are quite different from those of Fe^{3+}, B-site ordered structures can be stabilized. In this case, all the nearest-neighbor bonds are formed simply between a Fe^{3+} ion and a Mo^{5+} ion. However, most 3d transition metal impurities are located at random sites as a point defect. Some of these impurities create midgap states which can largely influence optical and conduction properties of the material. To our knowledge, no systematic review on formation of midgap states due to impurities has been reported for $BiFeO_3$. In principle, the defect level is determined as a result of combined Coulomb potential of the number of positive charge in the nucleus, the number of electrons in the ion, the number of occupied d(t_{2g}) and d(e_g) orbitals, and the Madelung potential. Defect levels of various transition metal impurities in oxide compounds have been discussed.[54] The midgap states can be partially filled by band filling control and even charge trapping in an electric field. The electrons trapped in the defect sites can move to the conduction band through random thermal fluctuation and move freely before relaxing to a defect site. As often observed in transition metal oxides different from conventional semiconductors, band edge states can be still localized up to a certain level called a mobility edge due to randomness and polaronic self-localization. In this case, variable range hopping mechanisms are necessary to explain the electronic conduction.[55] Even at relatively low temperature, through the Poole–Frenkel mechanism,[56] electrons can hop to move among localized impurity sites in a large electric field.

On the other hand, understanding of magnetic properties in insulating compounds has been well established on the basis of the superexchange interaction. The essence of the superexchange interaction is related to whether or not the total energy can be lowered through intersite hopping ($d^n + d^n \rightarrow d^{n+1} + d^{n-1} \rightarrow d^n + d^n$) under the scheme of an effectively second order perturbation process when the corresponding spin configuration is given.[57] Ferromagnetic spin arrangement between the neighboring sites is favorable in terms of an on-site Hund rule unless the hopping is forbidden because of the Pauli exclusion principle. The exchange interaction

between the Fe^{3+} ions is such a case that half filled d^5 electrons cannot hop to a neighboring site without spin flipping when the magnetic moment of the ions are ferromagnetically aligned. In this case, antiferromagnetic spin alignment is favorable even if the energy $E(d^{n+1} + d^{n-1})$ of the intermediate state after the hopping is unstable in terms of the on-site Hund rule. With the background of a basic scheme of magnetic interactions, we will discuss the magnetic interaction between the host Fe^{3+} ion and several magnetic dopant ions.

Examples of B-site doping

A. Control of magnetism by Cr and Mn doping. One of the interesting dopants is Cr^{3+} which has three electrons in d orbitals producing a magnetic moment of 3 μ_B. The three electrons fill only t_{2g} orbitals and vacate e_g orbitals. The exchange interaction between Fe^{3+} and Cr^{3+} is ferromagnetic through half-filled e_g–empty e_g interaction (d^5–d^3 type). Although the Cr^{3+} ions do not meet each other at the nearest-neighboring sites in the limit of the small substitution ratio, the magnetic interaction between neighboring Cr^{3+} ions is weakly antiferromagnetic through half-filled t_{2g}–half-filled t_{2g} interaction. For the purpose of a ferromagnetic state, one needs to maximize the number of Fe^{3+}–Cr^{3+} bonds avoiding Fe^{3+}–Fe^{3+} bonds and Cr^{3+}–Cr^{3+} bonds. An ideal compound is a double perovskite of $BiFe_{0.5}Cr_{0.5}O_3$ in which Fe^{3+} and Cr^{3+} are G-type ordered making all bonds ferromagnetic d^5–d^3 type. But the double perovskite compound is not realized because the B-site ions are located randomly rather than ordered as a consequence of similar ionic radius and chemical valence state. If one can stabilize a superlattice structure by growing $BiFeO_3$ and $BiCrO_3$ one by one along [111] direction, a ferromagnetic ground state can be theoretically expected but it has not been reported yet. Another interesting impurity is an Mn^{3+} ion which has four electrons in d orbitals. The ion is Jahn–Teller active so local structural distortion associated with an anisotropic orbital (d_{3z2-r2}) can occur.[57] Provided that an oxygen octahedron surrounding the Mn^{3+} ion is elongated along the *z*-axis, magnetic interaction with a neighboring Fe^{3+} ion along the elongation (*z*-axis) is antiferromagnetic but the other principal axes result in ferromagnetic interaction. Although both Cr^{3+} and Mn^{3+} ions create ferromagnetic exchange interactions with neighboring Fe^{3+} ions, just dilute substitutions of the ions hardly stabilize a ferromagnetic state. Typical changes in the magnetic state generated by such random substitutions are to suppress the magnetic order and decrease the Néel temperature because of a magnetic frustration effect. In the limit of large magnetic frustration, we may expect spin/cluster glass behaviors at low temperature showing slow dynamics in magnetic responses.[58] The substitutions of magnetic impurities can be utilized in tuning the magnetic transition temperature so it happens at the same temperature as dielectric transition for enhancing magnetoelectric/magnetodielectric properties around the transition temperature.[59,60] To prevent magnetic frustration inevitable in the random substitutions, ordered structures of magnetic dopants, that is, new magnetic layers can be employed to study interfacial exchange coupling/bias with the $BiFeO_3$ through heteroepitaxial growth of bi-layers[61] or self-assembled composite structures like nano-pillars of $BiFeO_3$ and other spinel ferrites.[62]

B. Leakage current control and magnetic property tuning: Ti, Ni, Co and Mn doping. The concept of doping has also been applied to bismuth ferrite in an attempt to modify the electronic and magnetic properties and to reduce leakage currents.[63] B-site doping of BFO with Ti^{4+} has been shown to reduce leakage by over three orders of magnitude while doping with Ni^{2+} leads to a higher conductivity by over two orders of magnitude.[64] Likewise, doping with Cr or Mn has also been shown to greatly reduce leakage currents in BFO films.[65]

3.3 Oxygen-site substitution

It is well-known that BFO can lose oxygen, resulting in the formation of both bulk and surface vacancies. The presence of such oxygen vacancies, which can be achieved *e.g.* by controlling the growth parameters during thin film deposition,[66,67] changes both the electronic and chemical properties of BFO and, consequently, the performance of BFO devices. For example, oxygen vacancies have been shown to affect the electrochromic properties of $Bi_{0.9}Ca_{0.1}FeO_{3-0.05}$[68] and the tuning of domain wall conductivity. Studies of oxygen vacancy formation in bulk BFO suggest that vacancies can migrate from the bulk to the surface of the oxide. However, only limited attempts have been made to quantify the surface and bulk concentration of O-atom defects,[69] which is mainly due to experimental limitations to measure very small changes in oxygen content. Vacancies are also formed in bulk BFO by heating in vacuum or an oxygen deficient atmosphere or reducing gas. Ionic defects such as oxygen vacancies have their most pronounced effect on transport properties, that is ionic and electronic conductivity and diffusion.

Example of oxygen vacancy doping – controlling domain wall conductivity. Recently, there has been a number of investigations showing interesting electrical transport properties at ferroelectric domain walls in $BiFeO_3$ and other ferroic materials.[15,16,70–82] Variable levels of local electrical conductance have been measured at ferroelectric domain walls in $BiFeO_3$, hexagonal $YMnO_3$ and $Pb(Zr_{0.2}Ti_{0.8})O_3$. Such interfaces locally break the symmetry, induce stress, and vary the bonding between ions. This in turn gives rise to changes in bandwidth, orbital interactions and level degeneracy, opening venues for modifying the electronic structure of these strongly correlated materials. Charge transfer can induce carrier densities that are different at the interface than in the bulk, resulting in physical properties at the interface which may be completely different from those of the parent bulk materials.[83–87] Tuning and controlling the physical properties of interfaces and domain boundaries by doping provides a new playground for research and offers a new nanoelectronics characterization platform for future nanotechnology.[88]

The changes in electronic structure that occur at ferroelectric (multiferroic) domain walls due to doping can lead to changes in transport behavior. Indeed, domain wall conductivity has been shown in different ferroic materials with different transport behavior: the domain walls of $BiFeO_3$ were found to be more conductive than the domains, while those of $YMnO_3$ were found to be more insulating or conductive depending on their orientation.[79,80]

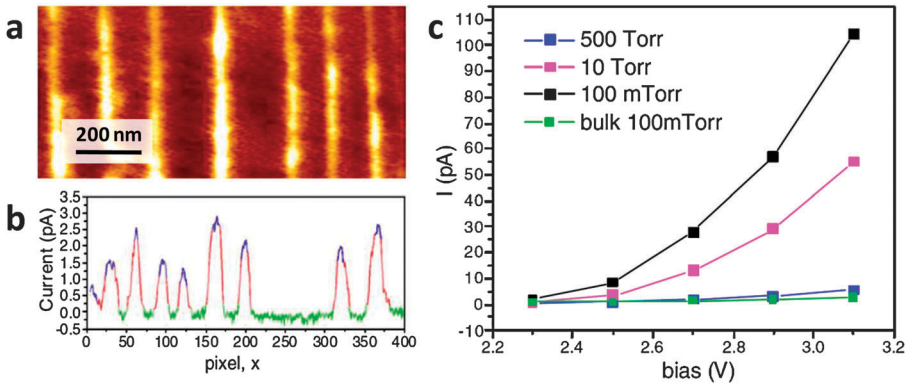

Fig. 6 (a) c-AFM images of a BFO sample with 109° stripe domains showing conduction at the walls. (b) Example of a c-AFM current image cross section. (c) Current levels for samples with different oxygen cooling pressure and thus varying density of oxygen vacancies.

The role of defect accumulation at the walls also deserves close scrutiny. Localized states are found in the spectrum of ferroelectric semiconductors, and states localized at the walls and inside the domain but close to the wall split off from the bulk continuum. These non-degenerate states have a high dispersion, in contrast to the "heavy-fermion" states at an isolated domain wall.[89] Charged double layers can be formed due to coupling between polarization and space charges at ferroelectric–ferroelastic domain walls.[90] Charged domain wall energies are about one order larger than the uncharged domain wall energies,[91] and phenomenological calculations show decoration of walls by defects such as oxygen vacancies. The presence of charge and defect layers at the walls means that such walls promote electrical failure by providing a high conductivity pathway from electrode to electrode.

The control of the electronic structure at walls by doping and strain in ferroelectric and ferroelastic oxides opens a way to effectively engineer nanoscale functionality in such materials.[92,93] Recently, the observation of tunable electronic conductivity at domain walls in La-doped BFO linked to oxygen vacancy concentration has been reported (Fig. 6). Specific growth conditions have been used to introduce varying amounts of vacancies in thin film samples.[94] The conductivity at 109° walls in such samples is thermally activated with activation energies of 0.24 to 0.5 eV. From a broader perspective, these results are a first step towards realizing the tantalizing possibility of inducing an insulator–metal transition locally within the confines of the domain wall through careful design of the electronic structure, the state of strain and chemical effects at the domain wall. For actual device applications the magnitude of the wall current needs to be increased. The choice of the right shallow-level dopant and host material might prove to be key factors in this respect. Further study of correlations between local polarization and conductivity is an exciting approach to understand the conduction dynamics and associated ferroelectric properties in the presence of strong coupling between electronic conduction and polarization in complex oxides.

4. Summary and outlook

In summary we have reviewed here exciting new physical phenomena in doped bismuth ferrite thin films underpinned by the drive to create new functional material systems. The multiferroic nature of bismuth ferrite makes it a unique case; doping not only leads to structure and polar order parameter modulation (like conventional ferroelectrics like PZT) but also controls the spin properties and gives rise to new transport phenomena not observed in the parent bismuth ferrite. From a structural order parameter perspective, we have recently shown that doping *via* rare-earths in bismuth ferrite induces a flexoelectric interaction, which eventually stabilizes complex modulated phases in the vicinity of the MPB through domain wall energy minimizations.[95] This is a radically new understanding of the origin of complex phases in the vicinity of an MPB, which opens new approaches where local order parameter competition can be exploited to realize giant electromechanical responses. The demonstration of polarization rotation *via* rare-earth substitution should motivate domain engineering experiments where crystallographic terminations are exploited to realize polarization rotation paths under an electric field. We have barely scratched the surface of physical possibilities; there is still a vast range of unexplored parameter space – *e.g.* can we demonstrate epitaxial stabilization of high polarization phases with the presence of magnetic order parameter frustration?

Nanoscale conduction phenomena in doped complex oxides form an exciting and growing field of interest in functional materials. Current breakthrough findings such as the discovery of conductive properties in ferroic domain walls have opened a number of new avenues and challenges, *e.g.* what sets the limits to the current transport behavior at walls: can one "design" the topological structure of the domain wall to controllably induce electronic phase transitions within the wall arising from the correlated electron nature? Is it possible to trigger an Anderson transition by doping of domain walls or straining them? The observation of superconductivity in ferroelastic walls of WO_3 certainly points to various exciting and unexplored areas of domain boundary physics triggered by doping.[96] An important aspect of multiferroic domain walls concerns the true state of magnetism at such a wall. Of interest is the effect of extra carriers introduced into the system, *e.g.*, by doping or electric gating, on magnetism. Is there a way to change the magnetic interaction from superexchange to double exchange?[97]

Doping-driven enhancement of functionality is also expected for the new tetragonal-like $BiFeO_3$ phase. The new structural phase of $BiFeO_3$ has been stabilized through heteroepitaxial strain. The phase is a metastable phase which has a highly-elongated

perovskite with large tetragonality ($c/a \sim 1.26$).[98,99] Regardless of large difference in lattice parameters, the highly-elongated phase can be transformed to the normal $BiFeO_3$ phase reversibly by applying the electric field leading to colossal electrostrain. Concurrent transition of the magnetic and ferroelectric order near room temperature has been reported.[36] Considering the delicate nature of phase competition in the strain-driven morphotropic phase boundary, we expect more chances to discover new functionality by doping studies of different structural variants of $BiFeO_3$.

From an application point of view, the ability to control the behavior of $BiFeO_3$ through chemical substitution in many different ways described in this article represents a large repertoire for engineering and fine-tuning its properties in order to satisfy specific device performance requirements. As a lead-free ferroelectric material with high polarization, $BiFeO_3$ has the potential to be used as the next generation material for FRAMs. Indeed, there have already been many reports of successful deposition of high quality $BiFeO_3$ films on top of Si. The next step in pursuing such devices perhaps is to explore reduction and control of the electric coercive field through doping, as is widely practiced in $Pb(Zr,Ti)O_3$. Reduction of leakage current through doping discussed above is particularly important. For bulk piezoelectric device applications, most of the bulk $BiFeO_3$ compounds available today are simply too conducting at room temperature. Only when this problem is solved, we will be able to take advantage of the high piezoelectric coefficient reported in $BiFeO_3$ for applications in sensors and actuators.

There are a number of novel-concept multiferroic devices which have been proposed to date including gated domain-wall conduction transistors, magnetic tunnel junctions with ferroelectric tunnel barriers, and electrically tunable exchange bias for MRAM devices. Exploration of such devices is the frontier in the multiferroic device community, and only the unique properties of multifunctional materials such as $BiFeO_3$ can make them a reality. However, integration and materials processing challenges for such novel heterostructured devices are likely to be formidable, and much fine-tuning of the delicate properties of $BiFeO_3$ through doping will perhaps be needed in order to take such concepts beyond the initial demonstration stage and turn them into useful electronic devices to be fabricated with high yield.

Acknowledgements

C.-H.Y. acknowledges support from the National Research Foundation of Korea (NRF) funded by the Ministry of Education, Science and Technology (contract no. 2010-0013528 and 2011-0016133). Work at Maryland was supported by the UMD-NSF-MRSEC (DMR 0520471), ARO W911NF-07-1-0410 and the W.M. Keck Foundation. Research at UNSW was supported by an ARC Discovery Project, NEDO and a DEST ISL grant. J.S. acknowledges support from a Future Fellowship Grant of the Australian Research Council (FT110100523).

References

1 R. Ramesh and N. A. Spaldin, *Nat. Mater.*, 2007, **6**, 21–29.
2 H. Ishiwara, *Curr. Appl. Phys.*, 2012, **12**, 603.
3 L. W. Martin, S. P. Crane, Y.-H. Chu, M. B. Holcomb, M. Gajek, M. Huijben, C.-H. Yang, N. Balke and R. Ramesh, *J. Phys.: Condens. Matter*, 2008, **20**(43), 434220.
4 Y. E. Roginska, Y. Y. Tomashpo, Y. N. Venevtse, V. M. Petrov and G. S. Zhdanov, *Sov. Phys. JETP*, 1966, **23**, 47.
5 S. V. Kiselev, R. P. Ozerov and G. S. Zhdanov, *Sov. Phys. Dokl.*, 1963, **7**, 742.
6 J. R. Teague, R. Gerson and W. J. James, *Solid State Commun.*, 1970, **8**(13), 1073.
7 J. Wang, J. B. Neaton, H. Zheng, V. Nagarajan, S. B. Ogale, B. Liu, D. Viehland, V. Vaithyanathan, D. G. Schlom, U. V. Waghmare, N. A. Spaldin, K. M. Rabe, M. Wuttig and R. Ramesh, *Science*, 2003, **299**, 1719–1722.
8 V. S. Filipeev, I. P. Smolyaninov, E. G. Fesenko and I. I. Belyaev, *Sov. Phys. Crystallogr.*, 1960, **5**, 913.
9 Y.-H. Chu, M. P. Cruz, C.-H. Yang, L. W. Martin, P.-L. Yang, J.-X. Zhang, K. Lee, P. Yu, L.-Q. Chen and R. Ramesh, *Adv. Mater.*, 2007, **19**(18), 2662.
10 Y. B. Chen, M. B. Katz, X. Q. Pan, R. R. Das, D. M. Kim, S. H. Baek and C. B. Eom, *Appl. Phys. Lett.*, 2007, **90**, 072907.
11 Y. H. Chu, Q. He, C.-H. Yang, P. Yu, L. W. Martin, P. Shafer and R. Ramesh, *Nano Lett.*, 2009, **9**(4), 1726–1730.
12 V. Shelke, D. Mazumdar, G. Srinivasan, A. Kumar, S. Jesse, S. Kalinin, A. Baddorf and A. Gupta, *Adv. Mater.*, 2011, **23**(5), 669–672.
13 R. Palai, *et al.*, *Phys. Rev. B: Condens. Matter Mater. Phys.*, 2008, **77**, 014110.
14 A. G. Gavriliuk, *et al.*, *Phys. Rev. B: Condens. Matter Mater. Phys.*, 2008, **77**, 155112.
15 J. Seidel, L. W. Martin, Q. He, Q. Zhan, Y. H. Chu, A. Rother, M. Hawkridge, P. Maksymovych, S. Kalinin, S. Gemming, P. Yu, N. Balke, M. Gajek, F. Wang, G. Catalán, J. F. Scott, N. A. Spaldin, J. Orenstein and R. Ramesh, *Nat. Mater.*, 2009, **8**, 229–234.
16 J. Seidel, P. Maksymovych, A. J. Katan, Y. Batra, Q. He, A. P. Baddorf, S. V. Kalinin, C.-H. Yang, J.-C. Yang, Y.-H. Chu, E. K. H. Salje, H. Wormeester, M. Salmeron and R. Ramesh, *Phys. Rev. Lett.*, 2010, **105**, 197603.
17 G. Catalan, J. Seidel, R. Ramesh and J. F. Scott, *Rev. Mod. Phys.*, 2012, **8**, 119–156.
18 J. M. Transcon, *et al.*, *Science*, 1987, **235**, 1373.
19 S. Jin, *et al.*, *Science*, 1994, **264**, 413.
20 B. Noheda, J. A. Gonzalo, L. E. Cross, R. Guo, S. E. Park, D. E. Cox and G. Shirane, *Phys. Rev. B: Condens. Matter Mater. Phys.*, 2000, **61**, 8687.
21 B. Jaffe, W. R. Cook and H. Jaffe, *Piezoelectric Ceramics*, Academic Press, London, 1971.
22 R. D. Shannon, *Acta Crystallogr., Sect. A: Cryst. Phys., Diffr., Theor. Gen. Cryst.*, 1976, **32**, 751.
23 G. Catalan and J. F. Scott, *Adv. Mater.*, 2009, **21**, 1–23.
24 A. M. Glazer, *Acta Crystallogr., Sect. A: Cryst. Phys., Diffr., Theor. Gen. Cryst.*, 1974, **31**, 756.
25 T. Shishidou, N. Mikamo, Y. Uratani, F. Ishii and T. Oguchi, *J. Phys.: Condens. Matter*, 2004, **16**, S5677.
26 R. Seshadri and N. A. Hill, *Chem. Mater.*, 2001, **13**, 2892.
27 N. A. Hill and A. Filippetti, *J. Magn. Magn. Mater.*, 2002, **242–245**, 976.
28 P. W. Anderson, *Phys. Rev.*, 1950, **79**, 350.
29 J. B. Goodenough, *Magnetism and the Chemical Bond*, John Wiley & Sons, New York, London, 1963.
30 M. Imada, A. Fujimori and Y. Tokura, *Rev. Mod. Phys.*, 1998, **70**, 1039–1263.
31 T. Moriya, *Phys. Rev.*, 1960, **120**, 91.
32 S. W. Cheong and M. Mostovoy, *Nat. Mater.*, 2007, **6**, 13.
33 J. Zhang, B. Xiang, Q. He, J. Seidel, R. Zeches, P. Yu, S.-Y. Yang, C.-H. Yang, Y.-H. Chu, L. W. Martin, A. M. Minor and R. Ramesh, *Nat. Nanotechnol.*, 2011, **6**, 98.
34 J. Zhou, M. Trassin, Q. He, N. Tamura, N. Kunz, C. Cheng, J. Zhang, W.-I. Liang, J. Seidel, C. Hsin, Y.-H. Chu and J. Wu, *J. Appl. Phys.*, 2012, **3**, 2905.
35 C.-H. Yang, J. Seidel, S. Y. Kim, P. B. Rossen, P. Yu, M. Gajek, Y.-H. Chu, L. W. Martin, M. B. Holcomb, Q. He, P. Maksymovych, N. Balke, S. V. Kalinin, A. P. Baddorf, S. R. Basu, M. L. Scullin and R. Ramesh, *Nat. Mater.*, 2009, **8**, 485–493.

36 K. T. Ko, M. H. Jung, Q. He, J. H. Lee, C. S. Woo, K. Chu, J. Seidel, B.-G. Jeon, Y. S. Oh, K. H. Kim, W.-I. Liang, H.-J. Chen, Y. H. Chu, Y. H. Jeong, R. Ramesh, J.-H. Park and C.-H. Yang, *Nat. Commun.*, 2011, **2**, 567.
37 M. Ramirez, A. Kumar, S. A. Denev, Y.-H. Chu, J. Seidel, L. Martin, S.-Y. Yang, R. Rai, X. Xue, J. F. Ihlefeld, N. Podraza, E. Saiz, S. Lee, J. Klug, S. W. Cheong, M. J. Bedzyk, O. Auciello, J. L. Musfeldt, D. G. Schlom, R. Ramesh, J. Orenstein and V. Gopalan, *Appl. Phys. Lett.*, 2009, **94**, 161905.
38 M. O. Ramirez, A. Kumar, S. Denev, N. Podraza and X. S. Xu, *et al.*, *Phys. Rev. B: Condens. Matter Mater. Phys.*, 2009, **79**, 224106.
39 M. O. Ramirez, M. Krishnamurthi, S. Denev, A. Kumar and S.-Y. Yang, *et al.*, *Appl. Phys. Lett.*, 2008, **92**, 022511.
40 Y.-P. Chiu, Y.-T. Chen, B.-C. Huang, M.-C. Shih, J.-C. Yang, Q. He, C.-W. Liang, J. Seidel, Y.-C. Chen, R. Ramesh and Y.-H. Chu, *Adv. Mater.*, 2011, **23**, 1530–1534.
41 S.-E. Park and T. R. Shrout, *J. Appl. Phys.*, 1997, **82**, 1804–1811.
42 R. Guo, L. E. Cross, S.-E. Park, B. Noheda, D. E. Cox and G. Shirane, *Phys. Rev. Lett.*, 2000, **84**, 5423.
43 Z. Kutnjak, J. Petzelt and R. Blinc, *Nature*, 2006, **441**, 956–959.
44 H. Fu and R. E. Cohen, *Nature*, 2000, **403**, 281–283.
45 L. Bellaiche, A. Garcia and D. Vanderbilt, *Phys. Rev. B: Condens. Matter Mater. Phys.*, 2001, **64**, 060103.
46 G. Catalan and J. F. Scott, *Adv. Mater.*, 2009, **21**, 2463–2485.
47 D. Lebeugle, D. Colson, A. Forget and M. Viret, *Appl. Phys. Lett.*, 2007, **91**, 022907.
48 S. Fujino, M. Murakami, V. Anbusathaiah, S.-H. Lim, V. Nagarajan, C. J. Fennie, M. Wuttig, L. Salamanca-Riba and I. Takeuchi, *Appl. Phys. Lett.*, 2008, **92**, 202904.
49 D. Kan, L. Palova, V. Anbusathaiah, C. J. Cheng, S. Fujino, V. Nagarajan, K. M. Rabe and I. Takeuchi, *Adv. Funct. Mater.*, 2010, **20**, 1108–1115.
50 C.-J. Cheng, D. Kan, V. Anbusathaiah, I. Takeuchi and V. Nagarajan, *Appl. Phys. Lett.*, 2010, **97**, 212905.
51 Y. Q. Jia, *J. Solid State Chem.*, 1991, **95**, 184.
52 D. Kan, V. Anbusathaiah and I. Takeuchi, *Adv. Mater.*, 2011, **23**, 1765–1769.
53 K. L. Kobayashi, T. Kimura, H. Sawada, K. Terakura and Y. Tokura, *Nature*, 1998, **395**, 677.
54 P. A. Cox, *Transition Metal Oxides*, Clarendon Press, Oxford, 1955.
55 N. F. Mott, *Philos. Mag.*, 1969, **19**, 835.
56 J. Frenkel, *Phys. Rev.*, 1938, **54**, 647.
57 K. I. Kugel and D. I. Khomskii, *Sov. Phys. Usp.*, 1982, **25**, 231.
58 C.-H. Yang, T. Y. Koo, S.-H. Lee, C. Song, K.-B. Lee and Y. H. Jeong, *Europhys. Lett.*, 2006, **74**(2), 348.
59 C.-H. Yang, T. Y. Koo and Y. H. Jeong, *Solid State Commun.*, 2005, **134**(4), 299.
60 C.-H. Yang, S.-H. Lee, T. Y. Koo and Y. H. Jeong, *Phys. Rev. B: Condens. Matter Mater. Phys.*, 2007, **75**, 140104.
61 P. Yu, *et al.*, *Phys. Rev. Lett.*, 2010, **105**, 027201.
62 H. Zheng, *et al.*, *Science*, 2004, **303**, 661.
63 Y.-H. Lee, J.-M. Wu and C.-H. Lai, *Appl. Phys. Lett.*, 2006, **88**, 042903.
64 X. Qi, J. Dho, R. Tomov, M. G. Blamire and J. L. MacManus-Driscoll, *Appl. Phys. Lett.*, 2005, **86**, 062903.
65 J. K. Kim, S. S. Kim, W.-J. Kim, A. S. Bhalla and R. Guo, *Appl. Phys. Lett.*, 2006, **88**, 132901.
66 M. L. Scullin, J. Ravichandran, C. Yu, M. Huijben, J. Seidel, A. Majumdar and R. Ramesh, *Acta Mater.*, 2010, **58**, 457.
67 M. L. Scullin, C. Yu, M. Huijben, S. Mukerjee, J. Seidel, Q. Zhan, J. Moore, A. Majumdar and R. Ramesh, *Appl. Phys. Lett.*, 2008, **92**, 202113.
68 J. Seidel, W. Luo, S. J. Suresha, P.-K. Nguyen, A. S. Lee, S.-Y. Kim, C.-H. Yang, J. Pennycook, S. T. Pantelides, J. F. Scott and R. Ramesh, *Nat. Commun.*, 2012, **3**, 799.
69 J. Seidel, *et al.*, submitted.
70 J. Seidel, G. Singh-Bhalla, Q. He, S.-Y. Yang, Y.-H. Chu and R. Ramesh, Phase Transitions, in print, DOI:10.1080/01411594.2012.695371.
71 A. Lubk, M. D. Rossell, J. Seidel, Q. He, S. Y. Yang, Y. H. Chu, R. Ramesh, M. J. Hÿtch and E. Snoeck, *Phys. Rev. Lett.*, 2012, **109**, 047601.
72 A. Y. Borisevich, O. Ovchinnikov, H. J. Chang, M. Oxley, P. Yu, J. Seidel, E. A. Eliseev, A. N. Morozovska, R. Ramesh, S. J. Pennycook and S. V. Kalinin, *ACS Nano*, 2010, **4**, 6071.
73 S.-Y. Yang, J. Seidel, S. J. Byrnes, P. Shafer, C.-H. Yang, M. D. Rossell, P. Yu, Y.-H. Chu, J. F. Scott, J. W. Ager III, L. W. Martin and R. Ramesh, *Nat. Nanotechnol.*, 2010, **5**, 143–147.
74 J. Seidel, D. Fu, S.-Y. Yang, E. Alarcòn-Lladò, J. Wu, R. Ramesh and J. W. Ager, *Phys. Rev. Lett.*, 2011, **107**, 126805.
75 J. Seidel, S.-Y. Yang, E. Alarcòn-Lladò, J. W. Ager and R. Ramesh, *Ferroelectrics*, 2012, **433**, 123.
76 P. Maksymovych, J. Seidel, Y.-H. Chu, A. Baddorf, P. Wu, L.-Q. Chen, S. V. Kalinin and R. Ramesh, *Nano Lett.*, 2011, **11**, 1906–1912.
77 Q. He, C.-H. Yeh, J.-C. Yang, G. Singh-Bhalla, C.-W. Liang, P.-W. Chiu, G. Catalan, L. W. Martin, Y.-H. Chu, J. F. Scott and R. Ramesh, *Phys. Rev. Lett.*, 2012, **108**, 067203.
78 S. Farokhipoor and B. Noheda, *Phys. Rev. Lett.*, 2011, **107**, 127601.
79 T. Choi, Y. Horibe, H. T. Yi, Y. J. Choi, W. Wu and S.-W. Cheong, Switchable ferroelectric diode and photovoltaic effect in $BiFeO_3$, *Nat. Mater.*, 2010, **9**(253), 63–66.
80 D. Meier, J. Seidel, A. Cano, K. Delaney, Y. Kumagai, M. Mostovoy, N. A. Spaldin, R. Ramesh and M. Fiebig, *Nat. Mater.*, 2012, **11**, 284–288.
81 G. Catalan, J. Seidel, R. Ramesh and J. F. Scott, *Rev. Mod. Phys.*, 2012, **8**, 119–156.
82 J. Seidel, Domain walls as nanoscale functional elements, *J. Phys. Chem. Lett.*, 2012, **3**, 2905.
83 S. B. Ogale, *Thin Films and Heterostructures for Oxide Electronics*, Springer, New York, 2005.
84 A. Ohtomo, D. A. Muller, J. L. Grazul and H. Y. Wang, *Nature*, 2002, **419**, 378–380.
85 E. Dagotto, *Science*, 2007, **318**, 1076–1077.
86 J. Mannhart and D. G. Schlom, *Science*, 2010, **327**, 1607–1611.
87 H. Yamada, Y. Ogawa, Y. Ishii, H. Sato, M. Kawasaki, H. Akoh and Y. Tokura, *Science*, 2004, **395**, 646–648.
88 P. Zubko, S. Gariglio, M. Gabay, P. Ghosez and J.-M. Triscone, *Annu. Rev. Condens. Matter Phys.*, 2011, **2**, 141–165.
89 B. G. Idlis, M. S. Usmanov and D. Parsons, *JETP Lett.*, 1992, **56**, 264–268.
90 Y. Xiao, V. B. Shenoy and K. Bhattacharya, *Phys. Rev. Lett.*, 2005, **95**, 247603.
91 M. Y. Gureev, A. K. Tagantsev and N. Setter, *18th IEEE ISAF Proceedings*, 2009, 37–42.
92 L. Goncalves-Ferreira, S. A. T. Redfern, E. Artacho, E. Salje and W. T. Lee, *Phys. Rev. B: Condens. Matter Mater. Phys.*, 2010, **81**, 024109.
93 W. Fan, J. Cao, J. Seidel, Y. Gu, J. W. Yim, C. Barrett, K. M. Yu, J. Ji, R. Ramesh, L. Q. Chen and J. Wu, *Phys. Rev. B: Condens. Matter Mater. Phys.*, 2011, **83**, 235102.
94 M. L. Scullin, J. Ravichandran, C. Yu, M. Huijben, J. Seidel, A. Majumdar and R. Ramesh, *Acta Mater.*, 2010, **58**, 457–463.
95 A. Y. Borisevich, E. A. Eliseev, A. N. Morozovska, C.-J. Cheng and J.-Y. Lin, *et al.*, *Nat. Commun.*, 2012, **3**, 77.
96 A. Aird and E. K. H. Salje, *J. Phys.: Condens. Matter*, 1998, **10**, L377–380.
97 M. Daraktchiev, G. Catalan and J. F. Scott, *Phys. Rev. B: Condens. Matter Mater. Phys.*, 2010, **81**, 224118.
98 R. J. Zeches, M. D. Rossell, J. X. Zhang, A. J. Hatt and Q. He, *et al.*, *Science*, 2009, **326**, 977–980.
99 H. Béa, B. Dupé, S. Fusil, R. Mattana and E. Jacquet, *et al.*, *Phys. Rev. Lett.*, 2009, **102**, 217603.

